Mem. S.A.It. Vol. 7, 182

Memorie della
Supplementi

Whistler Wave-Particle Interaction in a Temperate Ionosphere-like Plasma

A. R. Ellingboe

Plasma Research Laboratory National Centre for Plasma Science and Technology, Dublin City University, Dublin 9, Ireland, e-mail: bert.ellingboe@dcu.ie

Abstract. Whistler waves are produced when beam electrons, produced by a lightning strike near one of earths magnetic poles, approach the opposite pole and the associated increase in magnetic field. Bound whistlers, called 'helicon waves', have been used to produce high-density, large-area plasmas. The nature of the wave-plasma interaction has received considerable investigation. Particularly contentious has been experimental verification of production of beams of hot electrons in an opposite-analogous method to the formation of whistlers. Measurements of the plasma-wave-fields and rf-phase-resolved optical emission spectroscopy has been used to demonstrate that bunched electrons are produced, and that the electrons propagate axially resonant with the propagating EM wave.

Key words. Plasma Source – Helicon Waves – Wave particle interaction – Phase resolved optical emission spectroscopy

1. Introduction

The development of radio-frequency communication in the first half of the 20th century led to the first understanding of the earths upper atmosphere including the interaction with the solar wind resulting in the aurora, and over-the-horizon radio-communication via reflection off the ionosphere. Early radio communication was fraught with anomalous signals, including 'Whistling' sounds – ascending tones starting in the low kilo-hertz and increasing above the audible limit. These signals were later identified as resulting from a burst of electrons originating near a magnetic pole traversing along the earths magnetic field. Near the poles the magnetic field increases, and the electron burst would result in electromagnetic waves which were picked up by the radio receivers. The waves were labeled 'Whistlers' and were later identified as low- frequency waves (below the plasma frequency) in which the hall-term dominates Ohm's law. In the late 1950's solid state physicists began using radio frequencies to measure the Hall coefficient of magnetized semiconductors. Early theoretical investigations done by Aigrain (1960) determined that when the Hall term dominated Ohm's law ($\omega_{rf} < \omega_{ce} < \omega_{pe}$), the lines of force were helical. He coined the name 'helicon' to describe the associated waves. Shortly thereafter helicon standing waves were measured in cryogenic sodium (Rose et al. 1962). Both theoretical (Klozenberg et al. 1965; Legéndy 1964) and experimental (Facey & Harding 1966) reports on the effects of boundary conditions on the wave dispersion were published. The work

Send offprint requests to: A. R. Ellingboe

by Klozenberg et al. (1965) solved for helicon waves in a plasma with both conductive and insulating boundary conditions. Lehane & Thoneman (1965) confirmed this theory by propagating helicon waves in an *rf* maintained cylindrical plasma. In the late 1960's Boswell, studying wave propagation in a low pressure magneto-plasma, noticed that the helicon wave could be used to start and sustain the discharge, and the helicon plasma source was born (Boswell 1968). He measured standing helicon waves close to the antenna, and noted that the ionization efficiency was high and that plasmas approaching 100% ionization were readily attainable. The high efficiency was initially attributed to Landau damping of the helicon waves, but the experimental results were not in agreement with this linearized analysis of wave-particle interaction (Boswell 1970).

The plasma downstream from the source was quiescent and was later used to produce quiescent plasmas for space physics (Boswell 1975; Boswell & Giles 1976; Boswell et al. 1982). In 1984 (Boswell & Henry 1985) a helicon source was used with SF_6 fill gas to etch silicon. The etch rates attained were very high, approximately 10 times that of typical commercial *rf* diode reactors used by the microelectronics fabrication industry. Since then many other groups have contributed to the efforts to understand the basic physics of helicon plasma sources and their application to plasma processing (see Boswell & Chen (1997); Chen & Boswell (1997) and references within).

Details of the wave-particle interaction, and the resultant power coupling and affect on plasma global properties have continued to receive considerable attention (Ellingboe et al. 1995; Ellingboe & Boswell 1996; Degeling et al. 1996; Molvik et al. 1997; Scharer et al. 2002).

2. Derivation of the Helicon wave

A fluid equation can be obtained from the Vlasov equation ((Spitzer 1962) Eqs. 2-4), and the linearized, modified Ohms law is

$$\boldsymbol{E} + \overrightarrow{v \times \mathrm{B_0}} - \frac{1}{\mathrm{n_0 e}} \overrightarrow{j \times \mathrm{B_0}} - \eta \boldsymbol{j} - \frac{\mathrm{m_e}}{\mathrm{n_0 e^2}} \frac{\delta \boldsymbol{j}}{\delta t} = 0 \quad (1)$$

where j is the plasma current and η is the plasma resistivity. In defining Eq. 1, the gravitational term has been dropped, the plasma pressure term has been dropped on assumption of a temperate plasma, and there is assumed to be be no steady-state electric field or current. Combined with Maxwell's equations and solving for the index of refraction, N, yields (Spitzer (1962) Eq. 3-44)

$$N^2 = \frac{c^2}{v_\phi^2} = 1 - \frac{\omega_{pe}^2}{\omega_{rf}^2 - \omega_{ce}\omega_{ci} \pm \omega_{rf}(\omega_{ce} - \omega_{ci})} \quad (2)$$

where using the '+' yields a wave co-rotating with the ions and the '-' yields a wave co-rotating with the electrons, and $v_\phi = \omega_{rf}/k$ is the phase velocity of the wave. Some algebra yields

$$N^2 \left[\frac{\omega_{ci}}{\omega} - \frac{\omega}{\omega_{ce}} - \frac{i\nu}{\omega_{ce}} \pm (-1) \right] = \frac{\omega_{pe}^2}{\omega_{ce}\omega} \left[\frac{1}{1 - v_\phi^2/c^2} \right] . \quad (3)$$

Each of these terms can be related back to the initial stating of the problem, and can be neglected (Christiansen 1969) under the following conditions: $[\frac{\omega_{ci}}{\omega}]$ corresponds to $\overrightarrow{V \times \mathrm{B_0}}$ and can be neglected when the frequency is large compared with the ion cyclotron frequency ($\omega >> \omega_{ci}$.); $[\frac{\omega}{\omega_{ce}}]$ corresponds to the electron inertia term and can be neglected when the frequency is small compared with the electron cyclotron frequency and the density is high ($\omega \ll \omega_{ce}$ and $\omega \ll \omega_{pe}$, respectively). $[\frac{i\nu}{\omega_{ce}}]$ corresponds to the conductivity term and can be neglected when the electron collision frequency is small compared to the electron cyclotron frequency ($\nu \ll \omega_{ce}$.); $[\frac{1}{1-v_\phi^2/c^2}]$ corresponds to the displacement current in Maxwell's equations and can be ignored if the wave velocity is much less than the speed of light ($v_g \ll c$.); and [(-1)] corresponds to the Hall term ($\overrightarrow{j \times \mathrm{B_0}}$) and gives rise to the helicon wave.

For the conditions $\omega_{ci} \ll \omega \ll \omega_{ce} < \omega_{pe}$ only the Hall term remains, and the dispersion relation takes the simple form

$$N^2 = \frac{\omega_{pe}^2}{\omega_{ce}\omega} . \quad (4)$$

This is the helicon approximation.

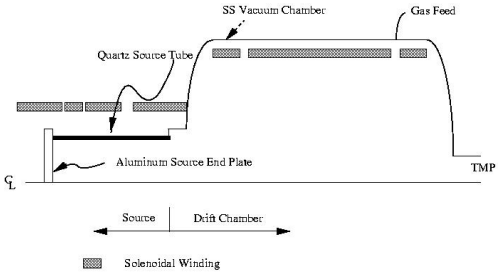

Fig. 1. The WOMBAT apparatus.

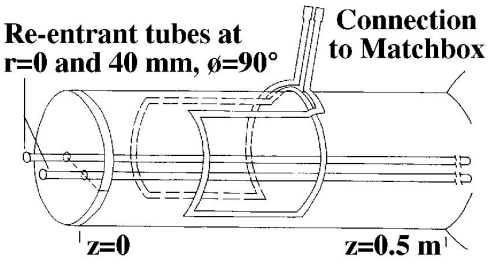

Fig. 2. The source region of WOMBAT, detailing the 'Boswell-type' antenna. Also shown are the re-entrant tubes at r=0 and 4 cm for probing by the optical periscope and B-dot probes, respectively.

3. Experiment

The WOMBAT apparatus consists of two regions, a drift chamber and a source (see Figure 1). The drift chamber is a stainless steel cylinder, 2 m long and 0.9 m diameter. The source is located on one end of the drift chamber, and is coaxial with the drift chamber. The source tube is made of a Pyrex tube, 180 mm inside diameter and 500 mm long. Both ends of the tube are open, one end opening into the drift chamber, and the other closed with an aluminum plate. On the end of the drift chamber opposite the source there is a Balzers 330 l/s turbo molecular pump to evacuate the chamber. A typical base pressure is 2.0×10^{-6} mTorr as measured with a cold-cathode gauge. Gas is fed into the WOMBAT vacuum chamber in the location shown in Figure 1 through a needle valve and the rate of flow is measured with a mass flow meter (typically 30 sccm). When gas is flowing, the pressure is measured with a capacitance manometer.

The apparatus is equipped with solenoidal windings which provide an axial background magnetic field (see Figure 1). The coils provide a uniform axial magnetic field (to within 5% at $r = 10$ cm) over the 500 mm axial extent of the source, then decreases monotonically over 500 mm axial extent to become uniform, in the drift chamber. Typical magnetic fields are 100 G (10 mT) in the source (run from 15 – 200 G) and 50 G (3.5 mT) in the drift chamber (run from 20 – 100 G).

Figure 2 shows a drawing of the source area, detailing the antenna and the re-entrant tubes.

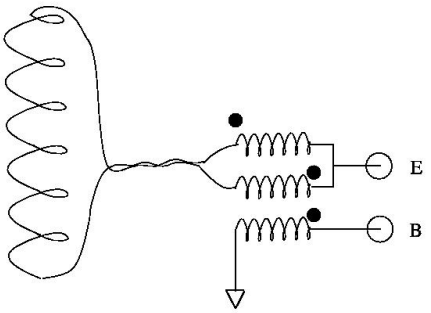

Fig. 3. Cartoon of a 5-turn B-dot probe, twisted pair wiring, and tri-filar winding for removing capacitive pickup (common-mode) from the B-dot signal (differential mode).

The *rf* magnetic wave-fields are measured using small inductive loops (B-dot probes) sensitive to the time varying magnetic fields associated with the plasma-wave-fields. Voltage is induced in the inductive loops according to Faraday's Law

$$V = \frac{d}{dt}(\boldsymbol{B}\cdot n\boldsymbol{A}), \tag{5}$$

where $\boldsymbol{B}$ is the *rf* magnetic field, $\boldsymbol{A}$ is the normal to the area enclosed by the loop with magnitude equal to the area enclosed by the loop, and n is the number of turns in the loop.

Typically, the probe-tip (the coil itself) is some distance away from the terminating resistance, and the two are connected with a

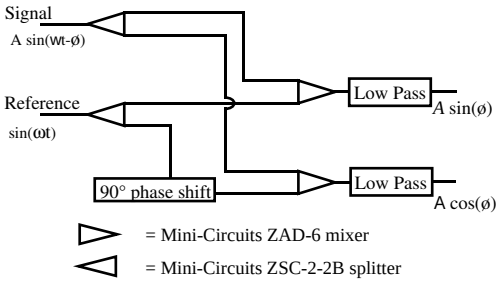

Fig. 4. The quadrature interferometer used for detecting amplitude and phase of the B-dot probe signal. The reference leg is fed by a Rogowski coil measuring the *rf* antenna current.

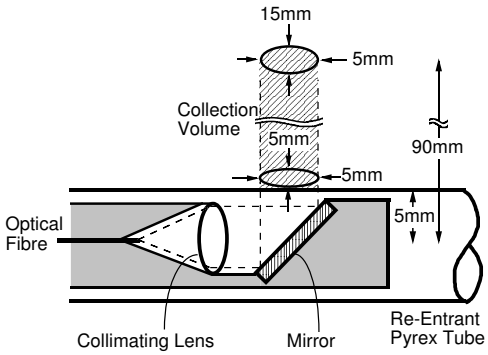

Fig. 5. Detail of the head of the optical periscope

transmission line, in this case a twisted pair. The coils are made from (US) 40 gauge magnet wire, and the same wire is used for the twisted pair and the hybrid combiner, as shown in Figure 3. Both E and B outputs (see Fig. 3) are terminated in 50 Ω.

Amplitude and phase of the B-dot signal are processed using the quadrature interferometer shown in fig. 4. The output filters had a single low-pass pole at 10 kHz which is a convenient frequency for most low-cost commercially available multi-channel digitizers. The absolute amplitude and phase difference can be calculated from

$$A = \sqrt{(A\sin\theta)^2 + (A\cos\theta)^2} \tag{6}$$

$$\theta = \arctan\left(\frac{A\sin\theta}{A\cos\theta}\right). \tag{7}$$

Phase-resolved optical emission spectroscopy (PROES) is used to investigate power deposition into plasma electrons as a function of phase within the *rf* cycle. If there is considerable interaction between the plasma-wave-fields and the electrons, then resonant electrons will be confined in phase by the interaction, and the phase of the peak of the interaction will advance with the wave as the wave propagates away from the antenna. The idea is to watch a fixed position in space and wait for the extra ionic (or perhaps atomic) excitation caused by "hot" electrons trapped in the wave passing through the light collection region.

To gain access to the source region, a re-entrant Pyrex tube is inserted through the aluminum end-plate (Figures 1 and 2) on the axis of the machine. The optical periscope is inserted into the re-entrant tube (Figure 5). By positioning the probe in z and Θ, light is collected from different volumes in the source region. The periscope collects light arriving from a radial sector of plasma. Because of lensing caused by the re-entrant tube which is curved in the Θ direction, the collection volume of the probe is 5 mm diameter circular at the probe tube, and elliptical with 5 mm axial by 15 mm Θ extent ellipse at the source tube wall (r = 90 mm.)

Light arriving from the collection volume is focused onto a fiber-optic bundle which guides the light out the end of the machine and into a 0.1 m monochromator tuned to the 443 nm ArII line. A photo-multiplier tube detects the photons. This line is chosen because its upper state is short lived (7 ns Vujnović & Wiese (1992)), and the line is easily separated from other emission lines. Photon arrival rates for this emission line are on the order of ten-thousand counts per second, which implies approximately 1 photon per 1000 *rf* cycles. For this reason, the quadrature interferometer can not be used to analyze the emission strength versus phase in the *rf* cycle and photon counting techniques are used instead. The signal from the photo-multiplier tube was used to start a time-to-amplitude converter (TAC) and a downward zero crossing from the antenna voltage probe was used to stop the TAC. Statistics of photon arrival versus *rf* phase were accumulated in a multi-channel-analyzer

(MCA). (A LeCroy model #3001 'QvT' TAC with integral MCA was used.)

Two types of plasma-wave-field electron interaction can be distinguish with the TOES technique. We make use of the fact that we are collecting light only from a *radial* sector, not a diameter, and assume $M = 1$ azimuthal mode structure for the E_z fields. If the upper state of the line we are detecting is being populated by bulk electrons involved with ohmic power transfer associated with the currents from a traveling helicon wave, then the modulation in signal would be at twice the fundamental frequency ($2f$) since locally the currents are equal in the $+\hat{z}$ and $-\hat{z}$ directions. If the electrons populating the upper state are produced by the large amplitude electric fields under the antenna and then remain phase-correlated with the wave as it propagates away from the antenna, then the modulation will be at the fundamental frequency. If the interaction is at $1f$, then the interaction *cannot* be a local phenomenon, but *must* be due to a long-time-scale interaction (history dependent.)

4. Experimental Data

4.1. Visual Observation

The first test was to visually observe the plasma with the naked eye. For example, with a Boswell antenna extending from $z = 18\,\text{cm}$ to $z = 33\,\text{cm}$ with 3.5 mTorr of Argon and magnetic field of 70 G, the following was observed. The power was slowly increased from zero Watts while looking through a window located on the axis in the end plate (see Figure 2.) At approximately thirty watts breakdown occurred. The plasma was diffuse and quite transparent - one could resolve probes which were located some distance downstream from the source. As the power was increased the intensity of plasma emission increased. There were regions of greater emission intensity close to the antenna. This is consistent with operation as an **E-mode** discharge because the power transfer is occurring in the plasma sheath around the antenna. At approximately three-hundred watts there was a distinct change in the plasma emission. This change will be found to be the **E** to **H-mode** transition. Above this transition, the overall emission intensity increased dramatically, and became edge dominant, and the bright spots near the antenna became more spread-out. Further increases in *rf* power resulted in increased emission intensity, with more emission at large radii than on axis; the emission profile was hollow. The probes which were clearly visible in **E-mode** were now obscured, due to increased emission intensity in the source as compared with light from downstream. The **E** to **H-mode** transition occurred over a small increase in power, but was step-wise continuous (although there was considerable hysteresis in power). These phenomena are consistent with **H-mode** discharges.

At fifteen-hundred watts there was a second change in the plasma emission. The emission intensity near the axis increased dramatically, and the radial profile was no longer hollow. These phenomena are consistent with **W-mode** power coupling. As well, objects interior to the plasma on the far end of the source were again resolvable: the emission intensity in the source was approximately the same, but there was a dramatic increase in emission intensity downstream from the source, which effectively 'back-lit' the objects. The increased optical emission in the diffusion chamber was suggestive of power deposition into the downstream region, presumably through the propagating helicon wave. This is only possible in a **W-mode** discharge.

4.2. Ion Saturation Current

Radial profiles of ion saturation current are shown in fig. 6. The bottom trace is for a low density, capacitive mode source operation. The second trace is an inductive mode; There are 'wings' at the radial positions were the fields lines trace back to the edges of the plasma source, and the power deposition in the source can be thought to be largely restricted to the edge region. The third trace corresponds to the same *rf* power as the second trace, but with the source operating in **W-mode**; The wings are still present, but there is an additional peak on-axis, consistent with power deposition by

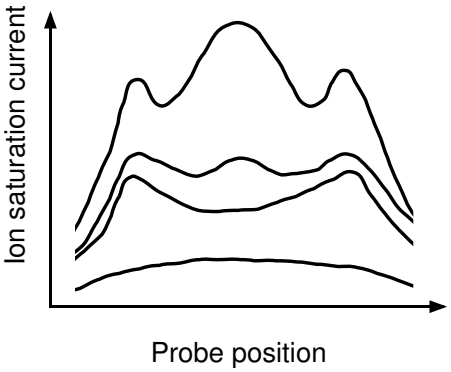

Fig. 6. Ion saturation current versus radial position across the diameter of the WOMBAT driftchamber. From bottom to top the four curves are for increasing power/ operational condition; 500 Watts (**E-mode**), 1600 Watts (**H-mode**), 1600 Watts (**W-mode**) and 2300 Watts (**W-mode**) (Ellingboe & Boswell 1996).

the axially-aligned wave currents arising from a partially electrostatic helicon wave (see text surrounding figs. 7 and 8.)

4.3. B-dot Probe Data

The transition in the Langmuir probe diameter scans occurring around 1600 Watts were surprising. The understanding of helicon source operation was that once the source was operating in inductive mode the dispersion relation for the helicon wave was well satisfied, and the propagating helicon wave would be responsible for at least some power deposition. Measurements of the axial profiles of the three components of the wave ($\mathbf{r}$, Θ, $\mathbf{z}$) just below (Fig. 7) and above (Fig. 8) the transition were made. Comparing traces from below and above the transition the $B_r$and $B_\theta$components are nearly identical: this is consistent with plasma density measurements in the source which show minimal increase in density in the source across this transition. The B_r and B_θ components are standing waves under the antenna and between the antenna and the conducting endplate, converting to traveling waves extending from the end of the antenna down into the diffusion chamber. Measurements at r=0 mm confirm that the wave has M=+1 polarization, as expected for a propagating helicon wave.

In sharp contrast, the B_z component changes dramatically from a low amplitude standing wave, with nulls close to the ends of the antenna to a very large amplitude standing wave under the antenna converting to a propagating wave downstream from the antenna. The wave maintains the same M=+1 polarization, but converts from a purely electromagnetic helicon wave, to a partially electrostatic helicon wave, gaining both magnetic and electric field components parallel to the axially magnetic field. Currents associated with the $E_z$field would be expected to be large, resulting in significant Ohmic heating. Also, individual energetic electrons with velocities close to the wave velocity can participate in resonant interaction with the wave.

4.4. Phase-Resolved Optical Emission Spectroscopy

The PROES data is interpreted assuming the following premise. The $4p^4D_{3/2}$ Argon ion excited state (the upper state of the 443 nm emission line being measured) can be produced by electron impact excitation from lower energy level states and decay from higher level states. The cross section for electron impact excitation of this excited state is not known, either experimentally or theoretically. For this discussion the cross section is assumed to be zero up to a threshold energy, whereupon it increases rapidly, flattens around 75 eV, and decreases slowly at energies greater than 75 eV. The threshold energy for this excitation is approximately 20 eV from the ground state ion and as little as 3 eV from ion metastable states. The lifetime of this excited state is 6.92 ns (Vujnović & Wiese 1992) with a small fraction of these excited ions undergoing the $4p^4D_{3/2} \rightarrow 4s^4P_{1/2}$ transition releasing a 443 nm photon. Fortunately, interpreting the TOES data does not rely on knowledge of the excitation cross section nor the species being excited.

As the helicon wave passes through the PROES collection volume shifting the EEDF, the number of electrons above the threshold en-

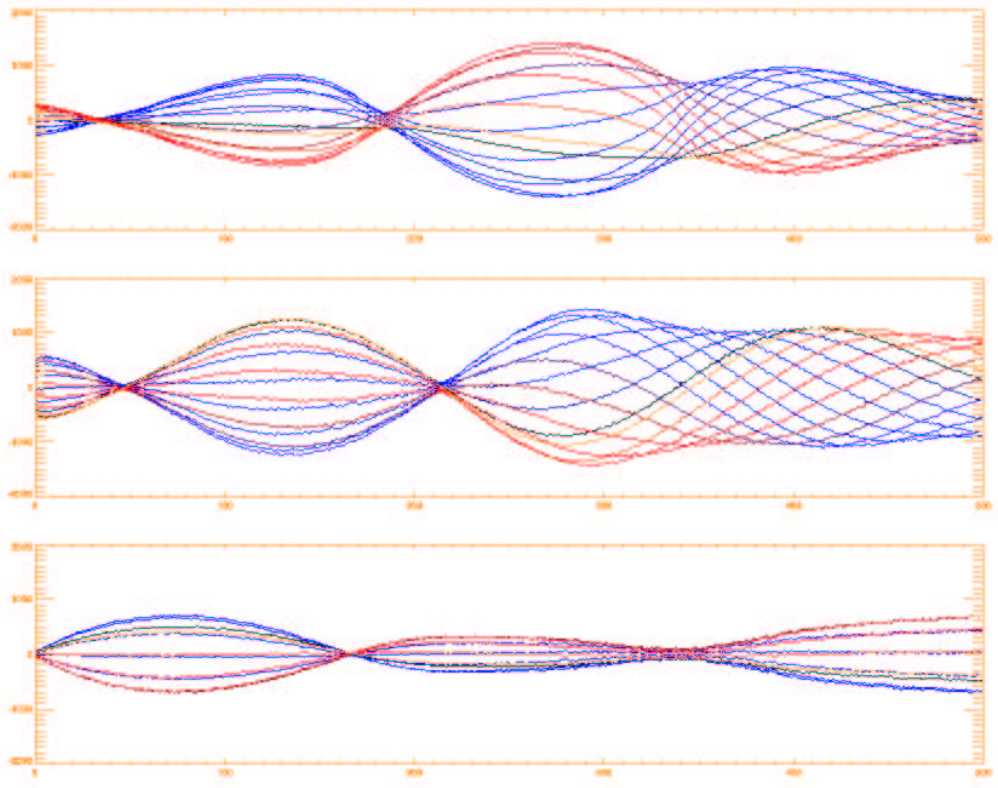

Fig. 7. Measurements of the *rf* magnetic field (B-dot) versus axial position at 1500 Watts, **H-mode** operation (Ellingboe & Boswell 1996). The plots represent radial (B_r), azimuthal (B-theta) and axial components (B_z). Overlay plots show advancing *rf* phase. Standing waves exist over the first 250 mm, and traveling waves for z > 250 mm. Note the low amplitude purely standing wave nature of the B_z component.

ergy changes. If these shifts in the EEDF are responsible for the oscillation in the TOES signal , two peaks per *rf* cycle would be seen, one when the EEDF shifts yielding current in the $+\hat{z}$ direction and a second peak when the EEDF shifts yielding current in the $-\hat{z}$ direction. In contrast, if there are electrons resonant with the wave, then the perturbation to the EEDF is only in the direction of propagation. This results in TOES signal fluctuation at the fundamental frequency ($1f$).

Figure 9 shows the PROES signal versus axial position; Overlaid is the relative phase of the B_z wave-field component. The time axis covers two *rf* cycles, the PROES data is duplicated for each *rf* cycle to allow comparison to the phase information.

Looking in detail, there are large amplitude peaks close to the antenna in the region of the large amplitude standing waves. The relative phase of adjacent peaks closely tracks the relative phase of the wave. Looking at the axially propagating wave (z>40 cm) there is a peak in PROES signal which closely tracks the relative phase of the B_z wave-field component. These observations confirm that the PROES signal is due to the propagating helicon wave. Further analysis shows that the oscillation in the PROES signal occurs at the fundamental frequency, not at $2f$, suggesting that the population of the upper state of the 443 nm transi-

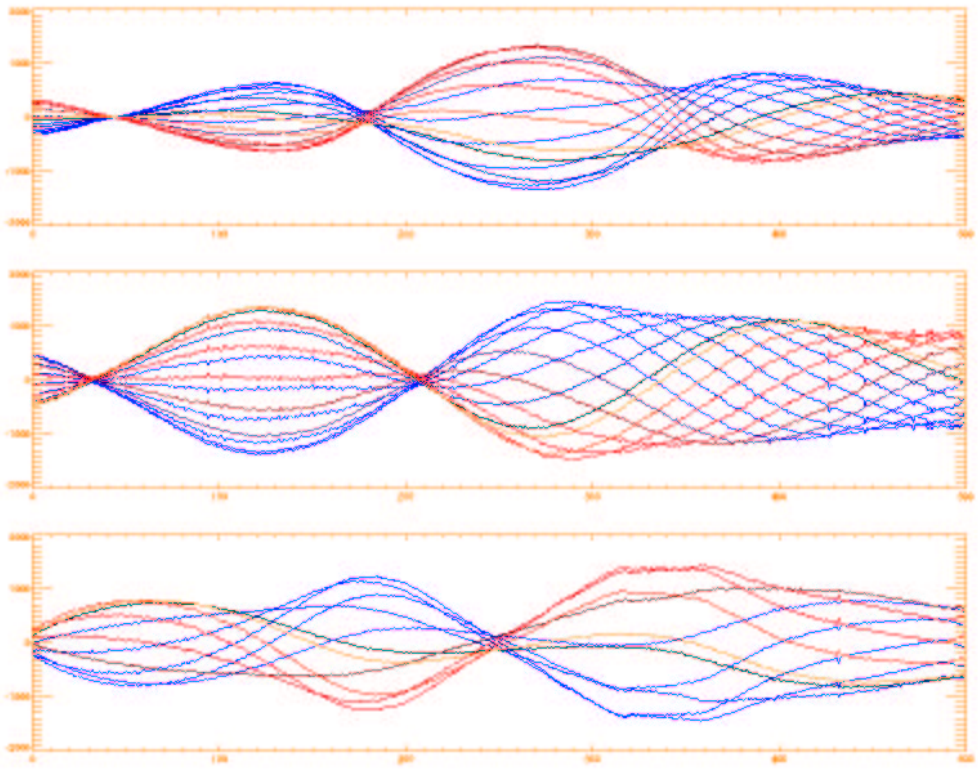

Fig. 8. Measurements of the *rf* magnetic field (B-dot) versus axial position at 1750 Watts, **W-mode** operation (Ellingboe & Boswell 1996). The plots represent radial (B_r), azimuthal (B_θ) and axial components (B_z). Overlay plots show advancing *rf* phase. Standing waves dominate over the first 250 mm, converting to traveling waves for z > 250 mm. Note the traveling wave in the B_z component; also the amplitude peak between z=300 mm and 400 mm has been 'clipped' by the electronics.

tion is caused by resonant electrons, not by the current associated with the propagating helicon wave.

5. Conclusions

The nature of power coupling in the WOMBAT helicon plasma source has been described. The mode-change occurring near 1600 Watts has been described as the transition from a purely electromagnetic helicon wave to a partially electrostatic helicon wave; The partially electrostatic helicon wave includes axially aligned components of both the wave magnetic field and electric field. Radial profiles of plasma density downstream of the helicon source show that the E_z fields contribute significantly to the power deposition on axis (away from the plasma edge), and with increasing power the fraction of on-axis heating increases. Analysis of the PROES data leads to the conclusion that wave-resonant electrons are produced in the source and propagate downstream with the partially-electrostatic helicon wave.

The observed wave-particle interaction is analogous, to the Whistler mode wave of the ionisphere. In the ionisphere, beams of hot electrons bunch together and as the magnetic field in the polar regions increases, the tone of the 'Whistler' changes; In the helicon plasma

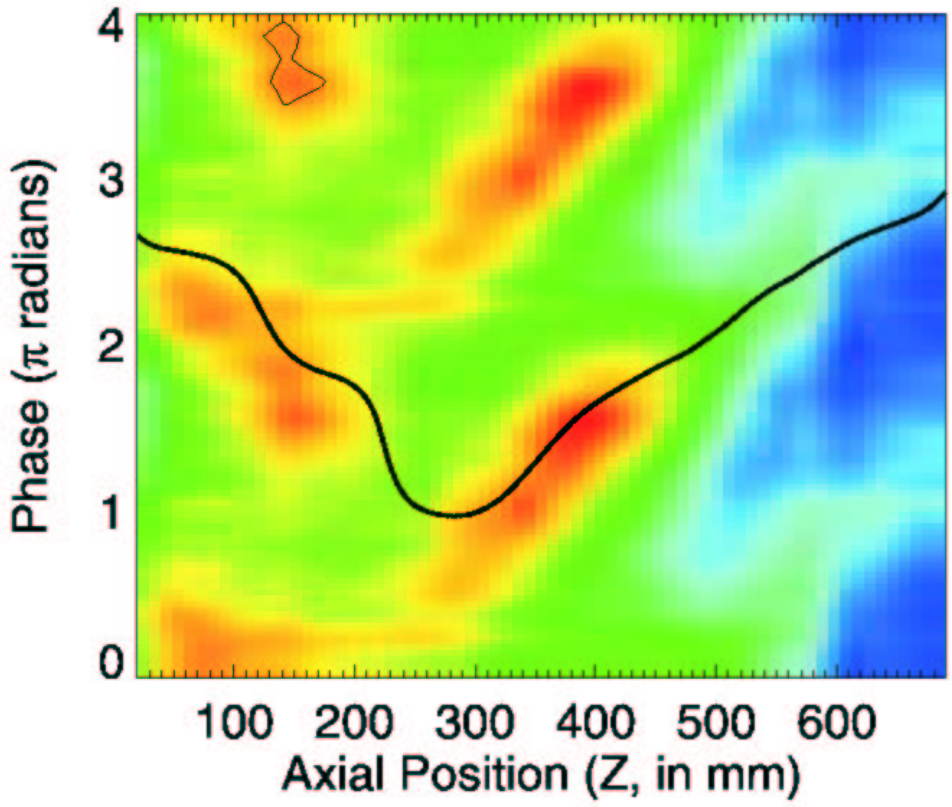

Fig. 9. Measurement of the Phase-Resolved Optical Emission Spectroscopy of the 443 nm Argon ion line versus axial position, note that is shown over 2-*rf* periods. The relative phase of the $B_z$component measured at r= 40 mm overlays the PROES contour.

source the tone is set by the *rf* generator. The helicon wave (a bounded Whistler wave) propagates along the plasma column according to the helicon dispersion relation 4 and when the conditions are right bunches of wave-resonant electrons are produced.

Acknowledgements. I would like to thank Rod Boswell for the freedom and support in my pursuit of the near-field interactions in helicon plasma sources, Nader Sadeghi and Jean-Paul Booth for support in establishing the PROES diagnostic, and Alex Degeling for collecting the final set of ion-saturation current measurements in the WOMBAT drift-chamber.

References

Aigrain, P. 1960, Proc. International Conference on Semiconductor Physics, Publishing House of the Czechoslovak Academy of Sciences, p.224, Prague

Boesgaard, A. M. et al. 1998, ApJ, 493, 206

Bonifacio, P. 2002, A&A, 395, 515

Bonifacio, P. et al. 2002, A&A, 390, 91

Boswell, R. W. 1968, Tech. Report, Flinders University of South Australia

Boswell, R. W. 1970, Physics Letters, 33A/7, 457

Boswell, R. W. 1970, PhD Thesis, Flinders University of South Australia

Boswell, R. W. 1975, Nature, 258/5530, 58

Boswell, R. W., & Giles, M. J. 1976, Physical Review Letters, 36/19, 1142

Boswell, R., Porteous, R., Prytz, A., Bouchoule, A., & Ranson, P. 1982, Physics Letters, 91A/4, 163
Boswell, R. W., & Henry, D. 1985, Appl. Phys. Lett., 47/10, 1095
Boswell, R. W., & Chen, F. F. 1997, IEEE TRANSACTIONS ON PLASMA SCIENCE, 25/6, 1244
Cayrel, R., Lebreton, Y., & Morel, P. 1999, Ap&SS, 265, 87
Chen, F. F., & Boswell, R. W. 1997, IEEE TRANSACTIONS ON PLASMA SCIENCE, 25/6, 1245
Christiansen, P. J. 1969, PhD Thesis, Flinders University of South Australia
Cuoco, A., et al. 2003, ArXiv Astrophysics e-prints, 7213
Degeling, A. W., Jung, C. O., Boswell, R. W., & Ellingboe, A. R. 1996, Phys. Plasmas, 6/3, 2788
Ellingboe, A. R., Boswell, R. W., Booth, J. P., & Sadeghi, N. 1995, Phys. Plasmas, 6/2, 1807
Ellingboe, A. R., & Boswell, R. W. 1996, Phys. Plasmas, 6/3, 2797
Facey, T. A., & Harding, G. N. 1966, Report CLM-R66, Culham Laboratory
King, J. R., et al. 1998, AJ, 115, 666
Klozenberg, J. P., McNamara, B., & Thonemann, P. C. 1965, J. Fluid Mech., 21, 545
Legéndy, C. R. 1964, Physical Review, 135/6A, 1713
Lehane, C. R., & Thoneman, P. C. 1965, Proc. of the Phys. Soc. of London, 85, 301
Molaro, P., & Pasquini, L. 1994, A&A, 281, L77
Molvik, A. W., Rognlien, T. D., & Ellingboe, A. R. 1997, PRL, 79/3, 233
Richard, O. et al. 2002, ApJ, 568, 979
Rose, F. E., Taylor, M. T., & Bowers, R. 1962, Phys. Rev., 127/4, 1122
Scharer, J., Degeling, A., Borg, G., & Boswell, R., 2002, Phys. Plasmas, 9/9, 3734
Spitzer, Lyman, Jr. 1962, Physics of Fully Ionized Gases, pub. John Wiley & Sons, Inc.
Vujnović, V., & Wiese, W. L. 1992, J. Phys. Chem. Ref. Data, 21/5, 919